Title: GABA-ergic dynamics in human frontotemporal networks confirmed by pharmaco-magnetoencephalography.

Abbreviated: GABA networks by pharmaco-MEG.

Authors: Natalie E. Adams[1], Laura E. Hughes[1,2], Holly N. Phillips[1], Alexander D. Shaw[2], Alexander G. Murley[1], David Nesbitt[1], Thomas E. Cope, W. Richard Bevan-Jones, Luca Passamonti, James B. Rowe[1,2]

[1] Department of Clinical Neurosciences, Cambridge Biomedical Campus, University of Cambridge, Cambridge, CB2 0QQ, UK

[2] MRC Cognition and Brain Sciences Unit, 15 Chaucer Road, Cambridge, CB2 7EF, UK

[3] Cambridge Centre for Ageing and Neuroscience (Cam-CAN), University of Cambridge, UK

Corresponding Author: James B. Rowe, james.rowe@mrc-cbu.cam.ac.uk

Number of Pages: 38
Number of Figures: 4
Number of Tables: 1
Number of Words for Abstract: 210
Number of Words for Introduction: 650
Number of Words for Discussion: 1489
Conflict of Interest: The authors declare no competing financial interests.

Acknowledgements: This work was funded by the Wellcome Trust (103838), the National Institute for Health Research Cambridge Biomedical Research Centre and the Medical Research Council (MC_U105597119; MC_U_00005/12; SUAG/004/91365), Cambridge Centre for Parkinson-plus and the Holt Fellowship. A.D.S is supported by a Wellcome Trust Strategic Award (104943/Z/14/Z).

Abstract

To bridge the gap between preclinical cellular models of disease and *in vivo* imaging of human cognitive network dynamics, there is a pressing need for informative biophysical models. Here we assess dynamic causal models (DCM) of cortical network responses, as generative models of magnetoencephalographic observations during an auditory oddball roving paradigm in healthy adults. This paradigm induces robust perturbations that permeate frontotemporal networks, including an evoked 'mismatch negativity' response and transiently induced oscillations. Here, we probe GABAergic influences of the networks using double-blind placebo-controlled randomised-crossover administration of the GABA re-uptake inhibitor, tiagabine (oral, 10mg) in healthy older adults. We demonstrate the facility of conductance-based neural mass mean-field models, incorporating local synaptic connectivity, to investigate laminar-specific and GABAergic mechanisms of the auditory response. The neuronal model accurately recapitulated the observed magnetoencephalographic data. Using parametric empirical Bayes for optimal model inversion across both drug sessions, we identify the effect of tiagabine on GABAergic modulation of deep pyramidal and interneuronal cell populations. We found a transition of the main GABAergic drug effects from auditory cortex in standard trials to prefrontal cortex in deviant trials. The successful integration of pharmaco- magnetoencephalography with dynamic causal models of frontotemporal networks provides a potential platform on which to evaluate the effects of disease and pharmacological interventions.

Significance Statement

Understanding human brain function and developing new treatments require good models of brain function. We tested a detailed generative model of cortical microcircuits that accurately reproduced human magnetoencephalography, to quantify network dynamics and connectivity in frontotemporal cortex. This approach identified the effect of a test drug (GABA-reuptake inhibitor, tiagabine) on neuronal function (GABA-ergic dynamics), opening the way for psychopharmacological studies in health and disease with the mechanistic precision afforded by generative models of the brain.

Introduction

Biophysically informed models of cognition and cognitive disorders facilitate the effective translation of the mechanisms and treatments of disease. Recent progress towards detailed generative models that replicate neurophysiological correlates of cognition based on cellular and network dynamics, such as 'Dynamic Causal Models' (DCM), make predictions that approximate observations by functional magnetic resonance imaging or electro- and magneto-encephalography (MEG) (Moran et al., 2013). To be most useful, these models should incorporate laminar, cellular and synaptic functions (Bastos et al., 2012), and adhere to basic principles of cortical connectivity (Shipp, 2016), while also being sufficiently tractable and accurate to study cognition.

The DCM framework developed to meet these criteria, with applications in health and neurological disorders (Kiebel et al., 2008; Stephan et al., 2008; Boly et al., 2011; Marreiros et al., 2015). DCMs draw on empirical priors for synaptic time constants and conductances, together with a mean-field forward model. They are optimised to match the observed neurophysiological data. DCMs are supported by extensive data for face-validity (Stephan et al., 2008, 2015) and construct-validity (Razi et al., 2015), but they must also achieve predictive validity (Moran et al., 2014; Gilbert and Moran, 2016; Shaw et al., 2018).

We tested the ability of DCMs to identify the effect of a pharmacological intervention. The DCMs were designed to model human frontotemporal cortical networks during an auditory oddball paradigm, with characteristic MEG responses to standard and deviant tones (<300ms). The differential response to these tones (the Mismatch Negativity, MMN) is abnormal in many neurological diseases (Boly et al., 2011; Naatanen et al., 2011; Hughes et al., 2013), reflecting a change in prediction errors in hierarchical frontotemporal networks (Garrido et al., 2009b; Phillips et al., 2015).

To examine laminar- and synaptic-dynamics in response to auditory stimuli we developed a new DCM with six cell populations, called "ext-DCM". In six connected regions (locations from Phillips et

al., 2015, 2016), we used a conductance-based mean-field cortical modelling scheme (cf. Moran et al., 2013; Marreiros et al., 2015). For auditory mismatch responses, both thalamocortical and cortico-cortical connections integrate feedforward sensory inputs and feedback expectations. The network architecture controls the flow and integration of information, via cell- and neurotransmitter-specific interactions. The ext-DCM introduces new cortico-thalamic burst-firing cells ('tp' in Figure 1a) that enable the model to generate beta activity from deep-layers (Roopun et al., 2008a, 2010; Bordas et al., 2015; Michalareas et al., 2016). The ext-DCM also separates the inhibitory interneuronal populations for superficial and deep pyramidal cells (e.g. Jiang *et al.*, 2015). These extensions improve the DCMs' functionality in terms of laminar dynamics. We tested the model's ability to accurately generate evoked magnetoencephalographic responses (i.e. event related fields, ERF), under placebo and drug conditions.

With the ext-DCM, we used the drug tiagabine to test how well the neurophysiological model could identify changes in the causes of observed neuronal dynamics. Tiagabine is a gamma-amino-butyric acid (GABA) re-uptake inhibitor. GABA is critical for the generation of physiological responses and rhythms in local and global processing (Whittington et al., 2000). This pharmacological specificity provides a more controlled acute test of DCMs than autoimmune (Symmonds et al., 2018) and genetic channelopathies (Gilbert et al., 2016).

Using parametric empirical Bayes to optimise the model across participants and drug conditions we examined how modelled GABAergic dynamics are altered by tiagabine. Based on the hypothesis that prediction and prediction error depend on short-term GABAergic plasticity (Castro-Alamancos and Connors, 1996; Garrido et al., 2009a; Mongillo et al., 2018; Spriggs et al., 2018), we predicted that upper and lower hierarchical frontotemporal processing would be differentially affected by tiagabine during standard and deviant tones.

In summary, the study's principal aims were i) to introduce and assess the ext-DCM for generating the event-related fields observed by MEG, ii) to identify receptor-specific changes that govern these dynamics, comparing tiagabine and placebo treatment conditions, and iii) to assess whether these

pharmacological effects are expressed dynamically across trial types and regions with laminar specificity.

Materials and Methods

Experimental Design:

We undertook a randomised placebo-controlled double-blind crossover study of the effects of tiagabine in 20 healthy adults (aged 67.5±4.2, ten male). Participants had no neurological or psychiatric illness and were recruited from the MRC Cognition and Brain Sciences and Join Dementia Research volunteer panels. The study was approved by the Cambridge Research Ethics Committee and written informed consent was acquired, in keeping with the declaration of Helsinki.

Neurophysiological responses were measured in an auditory roving oddball paradigm (Garrido et al., 2008). Binaural sinusoidal tones were presented in phase via ear-pieces for 75 ms (with 7.5ms ramp up and down at start and end of the tone), at 500 ms intervals. The frequency of the tone increased or decreased in steps of 50 Hz (range 400 – 800 Hz). The change of frequency occurred after between 3 and 10 repetitions, with a truncated exponential distribution that approximated a stable expectancy of change over time. Auditory thresholds were assessed in quiet at 500, 1,000, and 1,500 Hz. Tones were presented at 60dB above the average threshold for a standard population through the earpieces in the MEG.

Each participant attended two MEG sessions with a minimum two weeks interval. They received either 10 mg oral tiagabine or a placebo, in randomised order. Bloods were taken 105 minutes later, immediately prior to MEG data acquisition, to coincide with peak plasma levels and CNS penetration (Nutt et al., 2015).

Data Acquisition and pre-processing:

Magnetoencephalography (MEG) used a 306-channel Vectorview acquisition system (Elekta Neuromag, Helsinki) in a light Elekta Neuromag magnetically-shielded room. This consists of a pair of gradiometers and a magnetometer at each of 102 locations, sampled at 1000 Hz. Vertical and horizontal EOGs tracked eye movements and 5 head-position indicator coils tracked head position. A MEG-Compatible 70 channel EEG cap (Easycap GmbH) using Ag/AgCl electrodes positioned

according to the 10-20 system was used concurrently. A 3D digitizer (Fastrak Polhemus Inc., Colchester, VA) was used to record >100 scalp data points, nasion and bilateral pre-auricular fiducials. Subjects also underwent T1-weighted structural magnetic resonance imaging (MPRAGE sequence, TE = 2.9 msTR = 2000 ms, 1.1mm isotropic voxels) using a 3T Siemens PRISMA scanner.

MEG data pre-processing included head position alignment and movement compensation using 6 headcoils, placed around the head on the EEG cap, and employed the temporal extension of Signal Space Separation with MaxFilter v2.2 (Elekta Neuromag). The auto-detection of bad channels was combined with manual input of any channels logged as bad during data acquisition. The Statistical Parametric Mapping toolbox (SPM12) (The Wellcome Trust Centre for Neuroimaging, UCL, UK) was used for further pre-processing and analysis, in conjunction with modified and custom MATLAB scripts (MATLAB 2017a, Mathworks, Natick, MA). Data were Butterworth filtered between 1 and 180 Hz, epoched from -100 ms to 400 ms relative to the auditory stimuli and artefact rejected using EOG, EEG and MEG channel thresholding. Spectral analyses were performed using a multi-taper method. The deviant trial was taken as the 1st trial of a train, regardless of the frequency and the 6th trial of a train was modelled as 'standard'.

Source reconstruction used a forward model estimated using the single shell cortical mesh from each individual's T1-weighted MR structural scan. After co-registration using the fiducials and head points, local fields (LFs) for 6 sources of interest were source-reconstructed using SPM "COH" method, a combination of LORETA and minimum norm (Pascual-Marqui et al., 1994; Heers et al., 2016). Sources of interest were (with MNI coordinates in standard space following inverse normalisation): left auditory cortex (LAud; -42, -22, 7), left superior temporal gyrus (LSTG; -61 -32 8), left inferior frontal gyrus (LIFG; -46 20 8), right auditory cortex (RAud; 46, -14, 8), right superior temporal gyrus (RSTG; 59 -25 8) and right inferior frontal gyrus (RIFG; 46 20 8). To create images of induced power, SPM-LORETA was used for source localization of a 5 mm^3 regular grid at the MMN (150 – 250 ms) time window (100ms in width, regularization=0.05).

Correlation coefficients for comparing the actual and predicted ERFs were calculated using the corrcoef function (Pearson correlation) in MATLAB 2017a for each individual, condition and node.

Time-frequency analysis was performed in SPM12 using a multi-taper method with 100 ms windows overlapped by 5 ms and a bandwidth of 3. Frequency bands were split into alpha (8 – 13 Hz), beta (14 – 29 Hz), low gamma (30 – 48 Hz) and high gamma (52 – 80 Hz).

Neuronal Modelling: an extended canonical microcircuit model

We used conductance-based canonical mean field (CMM) models for evoked responses (Kiebel et al., 2008) utilising canonical microcircuit models (SPM12, DCM10). This approach to neurophysiologically informed modelling using DCM goes beyond descriptive biomarkers by providing a mechanistic link to realistic microscopic processes. A common approach in DCM is to invert the neuronal and spatial forward model as a single generative model, to solve the source reconstruction and biophysical modelling problems jointly by fitting the DCM to sensor data. However, we modelled source specific responses to suppress conditional dependencies between the neuronal parameters and the parameters of a spatial forward model. This affords more efficient estimators of neuronal parameters, providing the source reconstruction is sufficiently precise given the spatial topography of the network of interest. This has the advantage of compatibility with multiple studies of this task (Muthukumaraswamy et al., 2015; Gilbert and Moran, 2016; Shaw et al., 2017, 2018), including MEG and electrocorticography studies; the chosen network was based on the published bilateral A1, STG, IFG networks associated with the generation of the MMN response. Since this spatial element of the inverse problem was constrained, it is computationally more appropriate to source localise using SPM with prior expected sources. The subsequent DCM was then run on these virtual electrodes.

Our DCM included a conductance-based neural-mass model at each of the six anatomical locations, as shown in Figure 1. We compared the default 4-cell conductance canonical-microcircuit model with the ext-DCM, comprising 6 cell modules: a superficial pyramidal module (sp), a deep cortico-

cortical pyramidal module (dp), a thalamic-projection pyramidal module (tp), a granular stellate module (ss) and separate supragranular and infragranular interneuron populations (si & di). Excitatory autapses existed for all excitatory cell modules and all modules were also governed by an inhibitory self-gain function that provided tonic inhibition to each module. The ext-DCM was compared to the standard 4-cell model that is standard in SPM and is described in detail in Kiebel et al. (2008). In summary, the 4-cell DCM lacks thalamocortical connectivity and has a unitary inhibitory population interacting with all pyramidal and stellate cell populations.

The intrinsic connectivities are shown in Fig. 1a: note the excitatory conductances based on AMPA and NMDA and inhibitory GABA-A and GABA-B conductances. The model is an extension of the SPM conductance-based CMM model (SPM12, 2013): inclusion of separate supra- and infra-granular interneuron populations creates a more biophysically realistic model that allows a greater flexibility of independence of deep and superficial activity than in previous work (Bhatt et al., 2016; Shaw et al., 2018; Spriggs et al., 2018). Additionally, the new 'tp' population expressed a hyperpolarization-activated cation current (H-current) and a non-inactivating potassium current (M-current) to provide surrogate intrinsic dynamics involved in the characteristic intrinsic bursting behaviour of these cells. These two currents were fixed together with the reversal potential and the slope on the sigmoid convolution of in-activation for the H-current (details of which parameters had a permitted variance is given in Table 1). This, coupled with the cell capacitances, differentiates the intrinsic activation of the 'tp' population from the 'dp' population. The populations also differed in their extrinsic connectivities, with 'dp' populations forming cortico-cortical connections and 'tp' populations allowing for cortico-thalamocortical connections. The thalamus was modelled implicitly, by an 80 ms delay in connectivity with permitted variance.

Extrinsic connectivity between the six nodes is shown in Fig. 1b, with the detailed extrinsic population connections shown in Fig. 1c. In keeping with the established principle of differential cortical laminar projections of feed-forwards vs feedback connectivity (Bastos et al., 2012), backward connections are facilitated by the 'dp' cells terminating on 'sp' and 'si' cells, whilst forward

connections run from ‘sp’ cells to ‘ss’ cells. Cortico-thalamo-cortical connections originate from ‘tp’ cells and terminate following a thalamic delay at layer 4 ‘ss’ cells. The presence or absence of connections between nodes was based on the fully connected models from Phillips et al., (2015) and Shaw et al., (2019), which in turn were derived from Garrido et al., (2008). This was used for the basis of an iterative process to find the most likely reduced model (described below).

A Gaussian kernel (peak 60 ms, half-width 8 ms) represented auditory input to layer 4 stellates in bilateral auditory and inferior frontal cortex.

Bayesian Modelling and Statistical Analysis:

We used Bayesian model inversion (estimation) and Bayesian model comparison (selection) to identify the best explanation for subject-specific data, in terms of neuronal and biophysical parameters. Parametric Empirical Bayes (PEB) was used for group inferences and to examine drug effects, as described in Zeidman et al., (2019). By inverting a ‘full’ DCM per subject at the first level, PEB avoids the problem of different first level DCMs falling into different local optima, and allows subsequent comparison between conditions. At the second level, the parameters of interest were included in the PEB, namely the GABAA synaptic connections. This restricted set of second level parameters was oriented to our GABA-ergic hypothesis, and to improve stability of neural system identifiability.

The DCM was run for each subject. Data were filtered between 0–48 Hz and a Tukey window was applied that did not attenuate signals 50 ms before or 350 ms after stimuli. Inversion of the full model was run separately for the standard and deviant trials and the parameter distributions passed to second level Parametric Empirical Bayesian with contrasts for both trial types and drug conditions. All intrinsic and extrinsic AMPA, NMDA and GABA-A conductance scalings could vary independently in a manner that assumed symmetry between the two hemispheres. The prior means and permitted variances are summarised in Table 1.

Variational Bayesian statistics using the Laplace approximation determined the probable parameter space given the neuronal model and the data (Friston et al., 2007). The full model parameter space was reduced by iteratively searching for dependencies in this parameter space and systematically removing parameters not contributing to the free energy of the system (Henson et al., 2011). The optimised reduced model comprises all those parameters and connections found to contribute significantly to the system temporal dynamics. The comparison of full and reduced models is conceptually analogous to F-tests in classical statistics, but inferences are Bayesian. A second-level PEB was run, optimizing GABAA-ergic synaptic parameters (representing inhibitory gain). This second level PEB identifies parameter that are estimated to differ significantly between task conditions, or differ between drug-sessions, or for which there is a drug-by-condition interaction. The parameter distributions from this reduced model were used to create a Bayesian model average of parameters that differ significantly across the contrasts of trial types and drug conditions. The implementation of PEB for model optimisation and contrast estimation is summarised in Fig. 1e.

For other data types, Bayesian t-tests reported in the main text used JASP (JASP Team 2019, version 0.10.2). Frequentist statistical methods reported in the main text used MATLAB (2017a, Mathworks, Natick, MA).

Code Accessibility: The custom neuronal model used to generate these results is available at https://gitlab.com/tallie/edcm and works in conjunction with SPM12.

Results

Event related fields and induced spectral power

Event related responses to standard and deviant trials were in line with previous findings (Hughes and Rowe, 2013; Phillips et al., 2015, 2016) (Fig. 2a, first and second rows) and show the expected M100, the primary response after the onset of a tone (80-120 ms), a difference signal (MMN) between the standard and deviant trials (150-250 ms) and an M300 visible in frontal nodes (250-380 ms). The M100 was significantly reduced by tiagabine on standard and deviant trials, in left temporal nodes (A1, and STG $p<0.05$, paired t-test), whereas the later response leading into the M300 was significantly reduced only on deviant trials in L/R IFG ($p<0.05$, Bonferroni corrected for 6 regions).

The difference waveform (i.e. the deviant – the standard) reveals a typical biphasic MMN between 150-250ms, observed in primary auditory cortex and STG (Fig. 2a, third row). Tiagabine significantly reduced the second peak of the MMN ($p<0.05$) with bilateral IFG nodes and RSTG showing reductions in the first peak of the mismatch response on tiagabine ($p<0.05$). As with the deviant response, LIFG showed a significant reduction of the later MMN peak and the M300 on tiagabine ($p<0.05$).

The temporal profile of spectral power differences (see Methods for time-frequency analysis) matched that of the ERFs, including spectral counterparts to M100, MMN, continuing through the M300 window (Fig. 2b&c). During the M100, alpha-power (8-12 Hz) decreases on tiagabine were localized to temporal cortex and beta (14-29 Hz) decreases more prominently to posterior temporal cortex. During the MMN, increases in low and high gamma (30-48 Hz and 52-80 Hz respectively) were observed broadly across right frontal cortex, including IFG. Low gamma also showed increases in right temporal cortex.

Such changes in the observed spatiotemporal physiology on tiagabine will be dependent on changes in local and global network connectivity. The extended conductance-based dynamic causal model was therefore used to infer the causes of the observed physiological changes.

The Dynamical Causal Model:

The residuals (difference between the actual and generated ERFs) were greater (worse) for the 4-cell DCM than for the ext-DCM (Bayesian paired sample t-test: BF=8.5×10^{28}) as shown in Fig. 3a. Bayesian model comparison of the 4-cell *versus* ext-DCM confirmed that the ext-DCM performed better (ie. was a more likely generator of the observed MEG) than the 4-cell DCM (BF = 40.6, Figure 3b). Note that the model-evidences are corrected for differences in model complexity. Further analyses use the ext-DCM only.

Fig. 3c demonstrates the evoked-response generated by the conductance-based dynamic causal model at each node, for both drug conditions, using the optimal ext-DCM model as determined by Parametric Empirical Bayes (see methods). Fig. 3d shows the correlation between generated and observed data, for both standards' and deviants' responses, for both drug conditions at each node. Boxplots indicate the spread of single-subject correlations across the group (open circles are outliers), and black closed circles indicate the correlation of the mean response across all subjects for each condition and node. Note how the periods of difference between the placebo and drug conditions (black lines in Fig. 3c) are accurately generated (cf. 'predicted') by the model, with a high match to the observed data in Fig. 2a.

The modelled responses are explained in terms of the parameters of the optimised model. Using parametric empirical Bayes, condition effects on model parameters (connection and synaptic parameters) were compared across the standard and deviant conditions, as well as across the placebo and tiagabine conditions. Figure 4 shows the effect of tiagabine on the intrinsic GABAergic connectivity, assuming symmetry (three bilateral averaged nodes are shown). We confirmed that tiagabine significantly increases tonic GABAergic inhibition (posterior probability given for each parameter in Fig. 4a). This was seen primarily in the deep layer pyramidal and interneuron populations in primary auditory cortex and STG (Fig. 4a). An interaction between drug and condition was found for the deep interneurons of Auditory cortex (posterior $p \approx 1.0$).

Fig. 4b compares GABA-A conductance scaling on deep interneurons between placebo and tiagabine conditions, plotted for each individual. There was very strong evidence for differences between the two drug conditions in primary auditory areas for the standard condition (BF=782356), and in IFG and STG for the deviant condition (BF=3.58×10^7 & BF=166 respectively). This difference between primary auditory cortex and association cortex in STG/IFG, is in keeping with the functional differentiation of upper versus lower levels in a hierarchical neural network with backwards prediction and forward prediction error. Conversely, there was evidence of no difference between the two drug conditions for the standard condition in IFG (BF=0.274) and for the deviant condition in Aud (BF=0.241).

The correlation between tonic and phasic inhibition was explored for each region and condition. In the frontal cortex, a strong negative relationship was found between the tonic inhibition of deep inhibitory cells and their phasic inhibition onto cortico-thalamic cells (Fig. 4c Bayesian correlation pairs, BF=398.43).

Discussion

The principal insights from this study are that an extended conductance-based canonical mean-field method of dynamic causal modelling (a) succeeds in identifying the modulation of GABAergic dynamics by the GABA-reuptake inhibitor tiagabine, and (b) is tractable and an accurate generator of event-related fields that match those observed by magnetoencephalography, improving on an earlier 4-cell model. Moreover, the ext-DCM suggests the effect of drug to be both laminar-specific and dynamically modulated in different regions according to task condition. This opens the way for psychopharmacological studies in health and disease with the mechanistic precision afforded by using ext-DCMs as generative models.

We demonstrate that the intrinsic connectivity within hierarchical brain networks changes between conditions in the mismatch task. The approach is of generalised relevance to hierarchical network models of cognition such as speech (Cope et al., 2018), semantic (Adams et al., 2019) and visual perception (Muthukumaraswamy *et al.*, 2013). Moreover, the laminar and pharmacological specificity provided by the ext-DCM has the potential to quantify neuropathology in dementia, developmental and psychiatric disorders (Duyckaerts et al., 1986; Kinoshita et al., 1996; Ferrer, 1999; Ji et al., 2018; Shaw et al., 2018).

Understanding the MMN in terms of short-term plasticity.

Tiagabine modulated the GABA-egic dynamics across the trial types, implicating both local tonic- and phasic effects. Repetitive activation with the same stimulus attenuated the ERF (reduction in N1/N2 by 6^{th} repetition, Fig. 2). The model indicated higher tonic inhibition in the deep layers. We interpret this as local short-term plastic changes in deep-layer inhibition (Knott et al., 2002; Hensch, 2005; Jääskeläinen et al., 2007), regulating salient information (Mongillo et al., 2018).

The model suggested that tiagabine-induced increases of extracellular GABA leads to greater tonic inhibition, consistent with overspill of GABA onto extra-synaptic receptors (Semyanov et al., 2004). The effect was modulated differently in primary and associative processing areas: for tonic inhibition

of deep interneurons the drug's efficacy was highest in prefrontal cortex for deviant trials and in auditory cortex for standard trials. In other words, GABAergic effects are modulated differentially in upper and lower areas of the hierarchy dependent on the coding context. We speculate that this reflects differential emphasis on beliefs (& feedback predictions) *versus* feedforward sensory prediction errors in prefrontal versus primary auditory cortex; and that lower tonic inhibition at the presentation of a deviant tone relates to homeostatic competition between phasic and tonic inhibition (Wu et al., 2013). Increased phasic activation of deep-layer projections is necessary for feedback of top-down information on context, which in turn increases phasic (and decreased tonic) activation of deep interneurons. Decreasing tonic inhibition likely increases the interneuron population activation (Semyanov et al., 2004), leading to increased phasic inhibition onto deep pyramidal cells. This relationship was confirmed (Fig. 4c) between tonic inhibition of deep IFG interneurons and phasic inhibition of deep IFG thalamic-projection neurons. Figure 4b shows that whereas a drop in deep interneuron tonic inhibition was observed on deviant trials (*vs* standard), tiagabine abolished the effect. It is to be expected that increases in exogenous GABA would increase tonic GABAergic currents.

GABA-ergic modulation of evoked and induced responses.

Tiagabine affects oscillatory dynamics, which may influence behaviour (Coenen et al., 1995; Magazzini et al., 2016; Port et al., 2017; Wyss et al., 2017). It remains a challenge to relate systemic drug effects with local frequency-spectral phenomena. It has been proposed that beta-band activity is associated with infragranular cortical projection neurons with intrinsically bursting profiles (Groh et al., 2010; Roopun et al., 2010; Kim et al., 2015). We found that Tiagabine reduced the induced beta-band activity in temporal areas. The model suggests that tonic inhibition is increased on intrinsically bursting thalamic projection neurons in STG, which could increase rebound bursting via intrinsic M- and H-currents (Roopun *et al.*, 2008; Roopun *et al.*, 2008b).

Conversely, it has been shown that gamma-band activity is dependent on the GABA-A receptor activation and the phasic interplay of interneuron-pyramidal cell networks, particularly in the

363 superficial layers (Buffalo et al., 2011; Whittington et al., 2011). In the mismatch temporal window
364 (Fig. 2b) peak gamma increased occurring at the start of the mismatch period. This is consistent with
365 thalamic input (Di and Barth, 1992, 1993; Sukov and Barth, 2001) governing the envelope of gamma
366 activity in the superficial layers (Metherate and Cruikshank, 1999).

367 Overall, the observed dynamics and the model posterior parameters are consistent with knowledge
368 of network activation within the context of beta- and gamma- rhythm generation in cortex.

369 *Generative models of drug effects on cognitive physiology.*

370 Tiagabine's effect was largely confined to deep layers. As we modelled evoked activity it is difficult to
371 speculate on how this influences gamma activity across the network, however a reduction in deep-
372 layer influence may increase local cortical processing associated with gamma-band activity in the
373 superficial layers. As GABA levels are typically lower in older *versus* younger adults, tiagabine may
374 act 'restoratively'. This is corroborated with lower frequency responses that are dependent on GABA
375 (Mathias et al., 2001). Finally, we speculate that the reduced M100 on tiagabine results from the
376 widespread increased tonic inhibition represented in the model (Fig. 4), reducing local population
377 activity.

378 *Study limitations.*

379 Our study was motivated by the need for mechanistic studies of human cortical function, underlying
380 cognition, disease and therapeutics. Despite support for our three principal hypotheses, and
381 background validation studies (Moran et al., 2014), evidence from one study may not generalise to
382 other tasks and populations. There are study-specific considerations that limit our inferences, in
383 relation to our participants, our model, and drug of choice. For example, our participants were
384 healthy, and therefore have normal age related variance in GABA (Gao et al., 2013; Eavri et al.,
385 2018). They were older than those studied by Nutt et al (2015), and age-effects could interact with
386 the effects of tiagabine (Nutt et al., 2015). Our study was not designed to examine the effect of age

or ageing, but to focus on the normal brain in mid- and later-life. Further work would be required to examine the effects of ageing on the ext-DCM.

Our model provides a simplified substrate for the neurophysiological processes. It is more detailed than previous canonical microcircuit convolution models (Moran et al., 2013), in an effort to improve the modelling of specific dynamics from distinct cell populations, their differing connectivities, synaptic time constants and voltage-gated conductances. The extended model can produce a spectrum of fast and slow responses, with fast responses involved in local processing dominated by superficial layers and slower responses associated with feedback of information dominated by deep layers (Roopun et al., 2006; Kramer et al., 2008; Whittington et al., 2011). It can incorporate delayed activity associated with local, cortico-cortical and cortico-thalamo-cortical connections. Currently, this system is a simplified network acting as a neural mass, and can represent relevant cortical interactions involved in ERF generation in the context of this task and study. It does this by allowing forward and backward modulation of activity between deep and superficial layers, where synaptic time constants corroborate with standard GABA, NMDA and AMPA receptor decays. The six specified nodes are commonly cited in the literature in the context of this task (Garrido et al., 2009b; Phillips et al., 2015). Although they are not a complete representation of possible network configurations, they have been shown to capture critical aspects of cortical function: here the network has been supplemented with modelled exogenous and endogenous inputs via thalamus.

We emphasise Bayesian statistical analyses over classical frequentist methods. Where parameter estimates derived from earlier DCMs are used for frequentist statistical tests, they have excellent reliability across sessions, and similar power to fMRI and EEG studies (Rowe et al., 2010; Goulden et al., 2012; Bernal-Casas et al., 2013). Frequentist approaches are familiar to many readers, and have been the norm for comparison of ERFs, and we therefore include them selectively. Such a frequentist approach is surpassed by the direct inferences on posterior probability inherent in DCMs Bayesian inference, including PEB.

Tiagabine is a relatively specific blocker of GAT-1 at the concentrations used, but does not distinguish between the mechanisms activated by GABA (Bowery et al., 1987; Mody and Pearce, 2004; Lee and Maguire, 2014). The timing of the magnetoencephalography coincided with expected peak plasma levels, but levels may vary between individuals and future studies could include levels as a covariate of interest, or model time-varying responses in relation to drug levels (Muthukumaraswamy et al., 2013b).

In conclusion, we have used a conductance-based model of cortical neuronal dynamics to study GABA-ergic interactions and probe laminar-specific physiological responses to tiagabine. The model accurately generated physiological data that matched the MEG responses and confirmed the effect of tiagabine on tonic GABA-A inhibitory gain within frontal and temporal cortical circuits. Our data provide support for mechanistic studies of neurological disorders, including but not limited to GABAergic impairments (Murley and Rowe, 2018). They also point to new approaches for experimental medicine studies in humans that aim for the laminar, cellular or synaptic precision made possible in new generations of dynamic causal models.

Acknowledgements

This work was funded by the Wellcome Trust (103838), the National Institute for Health Research Cambridge Biomedical Research Centre and the Medical Research Council (MC_U105597119 & MC_U_00005/12), Cambridge Centre for Parkinson-plus and Holt Fellowship. We thank the PSP Association & FTD Support Group for raising awareness of the study.

435 **References**

436 Adams NE, Teige C, Mollo G, Karapanagiotidis T, Cornelissen PL, Smallwood J, Traub RD, Jefferies E,
437 Whittington MA (2019) Theta/delta coupling across cortical laminae contributes to semantic
438 cognition. J Neurophysiol:jn.00686.2018 Available at:
439 https://www.physiology.org/doi/10.1152/jn.00686.2018 [Accessed January 31, 2019].

440 Bastos AM, Usrey WM, Adams RA, Mangun GR, Fries P, Friston KJ (2012) Canonical Microcircuits for
441 Predictive Coding. Neuron 76:695–711 Available at:
442 https://www.sciencedirect.com/science/article/pii/S0896627312009592 [Accessed January 15,
443 2019].

444 Bernal-Casas D, Balaguer-Ballester E, Gerchen MF, Iglesias S, Walter H, Heinz A, Meyer-Lindenberg A,
445 Stephan KE, Kirsch P (2013) Multi-site reproducibility of prefrontal–hippocampal connectivity
446 estimates by stochastic DCM. Neuroimage 82:555–563 Available at:
447 https://www.sciencedirect.com/science/article/pii/S1053811913006307 [Accessed March 1,
448 2019].

449 Bhatt MB, Bowen S, Rossiter HE, Dupont-Hadwen J, Moran RJ, Friston KJ, Ward NS (2016)
450 Computational modelling of movement-related beta-oscillatory dynamics in human motor
451 cortex. Neuroimage 133:224–232 Available at:
452 https://www.sciencedirect.com/science/article/pii/S1053811916001981#f0005 [Accessed
453 January 15, 2019].

454 Boly M, Garrido MI, Gosseries O, Bruno M-A, Boveroux P, Schnakers C, Massimini M, Litvak V,
455 Laureys S, Friston K (2011) Preserved Feedforward But Impaired Top-Down Processes in the
456 Vegetative State. Science (80-) 332:858–862 Available at:
457 http://www.ncbi.nlm.nih.gov/pubmed/21566197 [Accessed February 26, 2019].

458 Bordas C, Kovacs A, Pal B (2015) The M-current contributes to high threshold membrane potential
459 oscillations in a cell type-specific way in the pedunculopontine nucleus of mice. Front Cell

460 Neurosci 9:121 Available at:
461 http://journal.frontiersin.org/article/10.3389/fncel.2015.00121/abstract [Accessed March 1,
462 2019].

463 Bowery NG, Hudson AL, Price GW (1987) GABAA and GABAB receptor site distribution in the rat
464 central nervous system. Neuroscience 20:365–383 Available at:
465 https://www.sciencedirect.com/science/article/pii/0306452287900984 [Accessed September
466 11, 2018].

467 Buffalo EA, Fries P, Landman R, Buschman TJ, Desimone R (2011) Laminar differences in gamma and
468 alpha coherence in the ventral stream. Proc Natl Acad Sci U S A 108:11262–11267.

469 Castro-Alamancos MA, Connors BW (1996) Cellular mechanisms of the augmenting response: short-
470 term plasticity in a thalamocortical pathway. J Neurosci 16:7742–7756 Available at:
471 http://www.ncbi.nlm.nih.gov/pubmed/8922430 [Accessed June 19, 2018].

472 Coenen AML, Blezer EHM, van Luijtelaar ELJM (1995) Effects of the GABA-uptake inhibitor tiagabine
473 on electroencephalogram, spike-wave discharges and behaviour of rats. Epilepsy Res 21:89–94
474 Available at: https://www.sciencedirect.com/science/article/pii/0920121195000153 [Accessed
475 February 26, 2019].

476 Di S, Barth DS (1992) The functional anatomy of middle-latency auditory evoked potentials:
477 thalamocortical connections. J Neurophysiol 68:425–431 Available at:
478 http://www.ncbi.nlm.nih.gov/pubmed/1382119 [Accessed September 5, 2018].

479 Di S, Barth DS (1993) Binaural vs. monaural auditory evoked potentials in rat neocortex. Brain Res
480 630:303–314 Available at:
481 https://www.sciencedirect.com/science/article/pii/000689939390670I [Accessed September 5,
482 2018].

483 Duyckaerts C, Hauw J-J, Bastenaire F, Piette F, Poulain C, Rainsard V, Javoy-Agid F, Berthaux P (1986)

484 Laminar distribution of neocortical senile plaques in senile dementia of the alzheimer type.
485 Acta Neuropathol 70:249–256 Available at: http://link.springer.com/10.1007/BF00686079
486 [Accessed January 15, 2019].

487 Eavri R, Shepherd J, Welsh CA, Flanders GH, Bear M, Nedivi E (2018) Interneuron simplification and
488 loss of structural plasticity as markers of aging-related functional decline. J Neurosci:0808–
489 0818 Available at: http://www.ncbi.nlm.nih.gov/pubmed/30108129 [Accessed August 22,
490 2018].

491 Ferrer I (1999) Neurons and their dendrites in frontotemporal dementia. Dement Geriatr Cogn
492 Disord 10 Suppl 1:55–60 Available at: http://www.ncbi.nlm.nih.gov/pubmed/10436342
493 [Accessed August 22, 2018].

494 Friston K, Mattout J, Trujillo-Barreto N, Ashburner J, Penny W (2007) Variational free energy and the
495 Laplace approximation. Neuroimage 34:220–234 Available at:
496 https://www.sciencedirect.com/science/article/pii/S1053811906008822 [Accessed May 1,
497 2018].

498 Gao F, Edden RAE, Li M, Puts NAJ, Wang G, Liu C, Zhao B, Wang H, Bai X, Zhao C, Wang X, Barker PB
499 (2013) Edited magnetic resonance spectroscopy detects an age-related decline in brain GABA
500 levels. Neuroimage 78:75–82 Available at:
501 https://www.sciencedirect.com/science/article/pii/S105381191300339X [Accessed September
502 4, 2018].

503 Garrido MI, Friston KJ, Kiebel SJ, Stephan KE, Baldeweg T, Kilner JM (2008) The functional anatomy of
504 the MMN: a DCM study of the roving paradigm. Neuroimage 42:936–944 Available at:
505 https://linkinghub.elsevier.com/retrieve/pii/S1053811908006484 [Accessed January 8, 2019].

506 Garrido MI, Kilner JM, Kiebel SJ, Stephan KE, Baldeweg T, Friston KJ (2009a) Repetition suppression
507 and plasticity in the human brain. Neuroimage 48:269–279 Available at:
508 https://www.sciencedirect.com/science/article/pii/S1053811909006661 [Accessed January 8,

2019].

Garrido MI, Kilner JM, Stephan KE, Friston KJ (2009b) The mismatch negativity: a review of underlying mechanisms. Clin Neurophysiol 120:453–463 Available at: http://www.ncbi.nlm.nih.gov/pubmed/19181570 [Accessed May 1, 2018].

Gilbert JR, Moran RJ (2016) Inputs to prefrontal cortex support visual recognition in the aging brain. Sci Rep 6:31943 Available at: http://www.nature.com/articles/srep31943 [Accessed January 14, 2019].

Gilbert JR, Symmonds M, Hanna MG, Dolan RJ, Friston KJ, Moran RJ (2016) Profiling neuronal ion channelopathies with non-invasive brain imaging and dynamic causal models: Case studies of single gene mutations. Neuroimage 124:43–53 Available at: https://www.sciencedirect.com/science/article/pii/S1053811915007788 [Accessed July 8, 2019].

Goulden N, Elliott R, Suckling J, Williams SR, Deakin JFW, McKie S (2012) Sample Size Estimation for Comparing Parameters Using Dynamic Causal Modeling. Brain Connect 2:80–90 Available at: http://www.liebertpub.com/doi/10.1089/brain.2011.0057 [Accessed March 1, 2019].

Groh A, Meyer HS, Schmidt EF, Heintz N, Sakmann B, Krieger P (2010) Cell-Type Specific Properties of Pyramidal Neurons in Neocortex Underlying a Layout that Is Modifiable Depending on the Cortical Area. Cereb Cortex 20:826–836 Available at: http://www.ncbi.nlm.nih.gov/pubmed/19643810 [Accessed June 19, 2018].

Heers M, Chowdhury RA, Hedrich T, Dubeau F, Hall JA, Lina J-M, Grova C, Kobayashi E (2016) Localization Accuracy of Distributed Inverse Solutions for Electric and Magnetic Source Imaging of Interictal Epileptic Discharges in Patients with Focal Epilepsy. Brain Topogr 29:162–181 Available at: http://link.springer.com/10.1007/s10548-014-0423-1 [Accessed December 18, 2018].

533 Hensch TK (2005) Critical period plasticity in local cortical circuits. Nat Rev Neurosci 6:877–888
534 Available at: http://www.nature.com/articles/nrn1787 [Accessed August 22, 2018].

535 Henson RN, Wakeman DG, Litvak V, Friston KJ (2011) A Parametric Empirical Bayesian Framework for
536 the EEG/MEG Inverse Problem: Generative Models for Multi-Subject and Multi-Modal
537 Integration. Front Hum Neurosci 5:76 Available at:
538 http://journal.frontiersin.org/article/10.3389/fnhum.2011.00076/abstract [Accessed May 1,
539 2018].

540 Hughes LE, Ghosh BCP, Rowe JB (2013) Reorganisation of brain networks in frontotemporal
541 dementia and progressive supranuclear palsy. NeuroImage Clin 2:459–468 Available at:
542 https://www.sciencedirect.com/science/article/pii/S2213158213000302 [Accessed October 24,
543 2018].

544 Hughes LE, Rowe JB (2013) The Impact of Neurodegeneration on Network Connectivity: A Study of
545 Change Detection in Frontotemporal Dementia. J Cogn Neurosci 25:802–813 Available at:
546 http://www.mitpressjournals.org/doi/10.1162/jocn_a_00356 [Accessed January 15, 2019].

547 Jääskeläinen IP, Ahveninen J, Belliveau JW, Raij T, Sams M (2007) Short-term plasticity in auditory
548 cognition. Trends Neurosci 30:653–661 Available at:
549 https://www.sciencedirect.com/science/article/pii/S0166223607002585 [Accessed June 26,
550 2018].

551 Ji E, Samuel S, Leboyer M, Guevara M, Guevara P, Poupon C, Grigis A, Houenou J (2018) T145.
552 ALTERATIONS IN SUPERFICIAL WHITE MATTER IN THE FRONTAL CORTEX IN SCHIZOPHRENIA: A
553 DWI STUDY USING A NOVEL ATLAS. Schizophr Bull 44:S172–S172 Available at:
554 https://academic.oup.com/schizophreniabulletin/article/44/suppl_1/S172/4957486 [Accessed
555 January 15, 2019].

556 Jiang X, Shen S, Cadwell CR, Berens P, Sinz F, Ecker AS, Patel S, Tolias AS (2015) Principles of
557 connectivity among morphologically defined cell types in adult neocortex. Science (80-)

558 350:aac9462–aac9462 Available at: http://www.ncbi.nlm.nih.gov/pubmed/26612957
559 [Accessed March 1, 2019].

560 Kiebel SJ, Garrido MI, Moran RJ, Friston KJ (2008) Dynamic causal modelling for EEG and MEG. Cogn
561 Neurodyn 2:121–136 Available at: http://link.springer.com/10.1007/s11571-008-9038-0
562 [Accessed January 14, 2019].

563 Kim EJ, Juavinett AL, Kyubwa EM, Jacobs MW, Callaway EM (2015) Three Types of Cortical Layer 5
564 Neurons That Differ in Brain-wide Connectivity and Function. Neuron 88:1253–1267 Available
565 at: https://www.sciencedirect.com/science/article/pii/S0896627315009812 [Accessed
566 September 4, 2018].

567 Kinoshita A, Tomimoto H, Tachibana N, Suenaga T, Kawamata T, Kimura T, Akiguchi I, Kimura J (1996)
568 A case of primary progressive aphasia with abnormally ubiquitinated neurites in the cerebral
569 cortex. Acta Neuropathol 92:520–524 Available at:
570 http://link.springer.com/10.1007/s004010050555 [Accessed January 15, 2019].

571 Knott GW, Quairiaux C, Genoud C, Welker E (2002) Formation of dendritic spines with GABAergic
572 synapses induced by whisker stimulation in adult mice. Neuron 34:265–273 Available at:
573 http://www.ncbi.nlm.nih.gov/pubmed/11970868 [Accessed January 3, 2019].

574 Kramer MA, Roopun AK, Carracedo LM, Traub RD, Whittington MA, Kopell NJ (2008) Rhythm
575 Generation through Period Concatenation in Rat Somatosensory Cortex Friston KJ, ed. PLoS
576 Comput Biol 4:e1000169 Available at: https://dx.plos.org/10.1371/journal.pcbi.1000169
577 [Accessed February 26, 2019].

578 Lee V, Maguire J (2014) The impact of tonic GABAA receptor-mediated inhibition on neuronal
579 excitability varies across brain region and cell type. Front Neural Circuits 8:3 Available at:
580 http://journal.frontiersin.org/article/10.3389/fncir.2014.00003/abstract [Accessed June 27,
581 2018].

582 Magazzini L, Muthukumaraswamy SD, Campbell AE, Hamandi K, Lingford-Hughes A, Myers JFM, Nutt
583 DJ, Sumner P, Wilson SJ, Singh KD (2016) Significant reductions in human visual gamma
584 frequency by the gaba reuptake inhibitor tiagabine revealed by robust peak frequency
585 estimation. Hum Brain Mapp 37:3882–3896 Available at:
586 http://www.ncbi.nlm.nih.gov/pubmed/27273695 [Accessed February 26, 2019].

587 Marreiros AC, Pinotsis DA, Brown P, Friston KJ (2015) DCM, Conductance Based Models and Clinical
588 Applications. In, pp 43–70. Springer, Cham. Available at: http://link.springer.com/10.1007/978-
589 3-319-20037-8_3 [Accessed January 15, 2019].

590 Mathias S, Wetter TC, Steiger A, Lancel M (2001) The GABA uptake inhibitor tiagabine promotes slow
591 wave sleep in normal elderly subjects. Neurobiol Aging 22:247–253 Available at:
592 http://www.ncbi.nlm.nih.gov/pubmed/11182474 [Accessed May 1, 2018].

593 Metherate R, Cruikshank SJ (1999) Thalamocortical inputs trigger a propagating envelope of gamma-
594 band activity in auditory cortex in vitro. Exp Brain Res 126:160–174 Available at:
595 http://link.springer.com/10.1007/s002210050726 [Accessed June 19, 2018].

596 Michalareas G, Vezoli J, van Pelt S, Schoffelen J-M, Kennedy H, Fries P (2016) Alpha-Beta and Gamma
597 Rhythms Subserve Feedback and Feedforward Influences among Human Visual Cortical Areas.
598 Neuron 89:384–397 Available at: http://www.ncbi.nlm.nih.gov/pubmed/26777277 [Accessed
599 March 1, 2019].

600 Mody I, Pearce RA (2004) Diversity of inhibitory neurotransmission through GABAA receptors.
601 Trends Neurosci 27:569–575 Available at:
602 https://www.sciencedirect.com/science/article/pii/S0166223604002279 [Accessed September
603 11, 2018].

604 Mongillo G, Rumpel S, Loewenstein Y (2018) Inhibitory connectivity defines the realm of excitatory
605 plasticity. Nat Neurosci 21:1463–1470 Available at: http://www.nature.com/articles/s41593-
606 018-0226-x [Accessed December 5, 2018].

607 Moran R, Pinotsis DA, Friston K (2013) Neural masses and fields in dynamic causal modeling. Front
608 Comput Neurosci 7:57 Available at:
609 http://journal.frontiersin.org/article/10.3389/fncom.2013.00057/abstract [Accessed January 3,
610 2019].

611 Moran RJ, Symmonds M, Dolan RJ, Friston KJ (2014) The Brain Ages Optimally to Model Its
612 Environment: Evidence from Sensory Learning over the Adult Lifespan Sporns O, ed. PLoS
613 Comput Biol 10:e1003422 Available at: https://dx.plos.org/10.1371/journal.pcbi.1003422
614 [Accessed February 26, 2019].

615 Murley AG, Rowe JB (2018) Neurotransmitter deficits from frontotemporal lobar degeneration. Brain
616 141:1263–1285 Available at: https://academic.oup.com/brain/article/141/5/1263/4823510
617 [Accessed October 24, 2018].

618 Muthukumaraswamy SD, Myers JFM, Wilson SJ, Nutt DJ, Hamandi K, Lingford-Hughes A, Singh KD
619 (2013a) Elevating Endogenous GABA Levels with GAT-1 Blockade Modulates Evoked but Not
620 Induced Responses in Human Visual Cortex. Neuropsychopharmacology 38:1105–1112
621 Available at: http://www.nature.com/articles/npp20139 [Accessed May 1, 2018].

622 Muthukumaraswamy SD, Myers JFM, Wilson SJ, Nutt DJ, Lingford-Hughes A, Singh KD, Hamandi K
623 (2013b) The effects of elevated endogenous GABA levels on movement-related network
624 oscillations. Neuroimage 66:36–41 Available at:
625 https://www.sciencedirect.com/science/article/pii/S1053811912010579?via%3Dihub
626 [Accessed February 26, 2019].

627 Muthukumaraswamy SD, Shaw AD, Jackson LE, Hall J, Moran R, Saxena N (2015) Evidence that
628 Subanesthetic Doses of Ketamine Cause Sustained Disruptions of NMDA and AMPA-Mediated
629 Frontoparietal Connectivity in Humans. J Neurosci 35:11694–11706 Available at:
630 http://www.ncbi.nlm.nih.gov/pubmed/26290246 [Accessed January 14, 2019].

631 Naatanen R, Kujala T, Kreegipuu K, Carlson S, Escera C, Baldeweg T, Ponton C (2011) The mismatch

negativity: an index of cognitive decline in neuropsychiatric and neurological diseases and in ageing. Brain 134:3435–3453 Available at: https://academic.oup.com/brain/article-lookup/doi/10.1093/brain/awr064 [Accessed February 26, 2019].

Nutt D, Wilson S, Lingford-Hughes A, Myers J, Papadopoulos A, Muthukumaraswamy S (2015) Differences between magnetoencephalographic (MEG) spectral profiles of drugs acting on GABA at synaptic and extrasynaptic sites: A study in healthy volunteers. Neuropharmacology 88:155–163 Available at: https://www.sciencedirect.com/science/article/pii/S0028390814003001 [Accessed January 3, 2019].

Pascual-Marqui RD, Michel CM, Lehmann D (1994) Low resolution electromagnetic tomography: a new method for localizing electrical activity in the brain. Int J Psychophysiol 18:49–65 Available at: http://linkinghub.elsevier.com/retrieve/pii/016787608490014X [Accessed December 18, 2018].

Phillips HN, Blenkmann A, Hughes LE, Bekinschtein TA, Rowe JB (2015) Hierarchical Organization of Frontotemporal Networks for the Prediction of Stimuli across Multiple Dimensions. J Neurosci 35:9255–9264 Available at: http://www.ncbi.nlm.nih.gov/pubmed/26109651 [Accessed May 1, 2018].

Phillips HN, Blenkmann A, Hughes LE, Kochen S, Bekinschtein TA, Cam-CAN, Rowe JB (2016) Convergent evidence for hierarchical prediction networks from human electrocorticography and magnetoencephalography. Cortex 82:192–205 Available at: https://www.sciencedirect.com/science/article/pii/S0010945216301058#fig3 [Accessed January 15, 2019].

Port RG, Gaetz W, Bloy L, Wang D-J, Blaskey L, Kuschner ES, Levy SE, Brodkin ES, Roberts TPL (2017) Exploring the relationship between cortical GABA concentrations, auditory gamma-band responses and development in ASD: Evidence for an altered maturational trajectory in ASD.

Autism Res 10:593–607 Available at: http://www.ncbi.nlm.nih.gov/pubmed/27696740 [Accessed February 26, 2019].

Razi A, Kahan J, Rees G, Friston KJ (2015) Construct validation of a DCM for resting state fMRI. Neuroimage 106:1–14 Available at: https://www.sciencedirect.com/science/article/pii/S1053811914009446 [Accessed September 13, 2018].

Roopun AK, Kramer MA, Carracedo LM, Kaiser M, Davies CH, Traub RD, Kopell NJ, Whittington MA (2008a) Period concatenation underlies interactions between gamma and beta rhythms in neocortex. Front Cell Neurosci 2:1 Available at: http://journal.frontiersin.org/article/10.3389/neuro.03.001.2008/abstract [Accessed January 3, 2019].

Roopun AK, Kramer MA, Carracedo LM, Kaiser M, Davies CH, Traub RD, Kopell NJ, Whittington MA (2008b) Temporal interactions between cortical rhythms. Front Neurosci 2:145–154 Available at: http://journal.frontiersin.org/article/10.3389/neuro.01.034.2008/abstract [Accessed January 3, 2019].

Roopun AK, LeBeau FEN, Rammell J, Cunningham MO, Traub RD, Whittington MA (2010) Cholinergic neuromodulation controls directed temporal communication in neocortex in vitro. Front Neural Circuits 4:8 Available at: http://journal.frontiersin.org/article/10.3389/fncir.2010.00008/abstract [Accessed June 19, 2018].

Roopun AK, Middleton SJ, Cunningham MO, LeBeau FEN, Bibbig A, Whittington MA, Traub RD (2006) A beta2-frequency (20-30 Hz) oscillation in nonsynaptic networks of somatosensory cortex. Proc Natl Acad Sci U S A 103:15646–15650 Available at: http://www.ncbi.nlm.nih.gov/pubmed/17030821 [Accessed February 26, 2019].

Rowe JB, Hughes LE, Barker RA, Owen AM (2010) Dynamic causal modelling of effective connectivity

682 from fMRI: Are results reproducible and sensitive to Parkinson's disease and its treatment?
683 Neuroimage 52:1015–1026 Available at:
684 https://www.sciencedirect.com/science/article/pii/S105381190901369X [Accessed March 1,
685 2019].

686 Semyanov A, Walker MC, Kullmann DM, Silver RA (2004) Tonically active GABAA receptors:
687 modulating gain and maintaining the tone. Trends Neurosci 27:262–269 Available at:
688 https://www.sciencedirect.com/science/article/pii/S0166223604000906?via%3Dihub
689 [Accessed June 18, 2018].

690 Shaw AD, Hughes LE, Moran RJ, Coyle-Gilchrist I, Rittman T, Rowe JB (2018) In vivo assay of cortical
691 microcircuitry in frontotemporal dementia: a platform for experimental medicine studies.
692 bioRxiv:416388 Available at: https://www.biorxiv.org/content/early/2018/09/13/416388.short
693 [Accessed November 7, 2018].

694 Shaw AD, Moran RJ, Muthukumaraswamy SD, Brealy J, Linden DE, Friston KJ, Singh KD (2017)
695 Neurophysiologically-informed markers of individual variability and pharmacological
696 manipulation of human cortical gamma. Neuroimage 161:19–31 Available at:
697 http://www.ncbi.nlm.nih.gov/pubmed/28807873 [Accessed January 14, 2019].

698 Shipp S (2016) Neural Elements for Predictive Coding. Front Psychol 7:1792 Available at:
699 http://journal.frontiersin.org/article/10.3389/fpsyg.2016.01792/full [Accessed January 14,
700 2019].

701 Spriggs MJ, Sumner RL, McMillan RL, Moran RJ, Kirk IJ, Muthukumaraswamy SD (2018) Indexing
702 sensory plasticity: Evidence for distinct Predictive Coding and Hebbian learning mechanisms in
703 the cerebral cortex. Neuroimage 176:290–300 Available at:
704 https://www.sciencedirect.com/science/article/pii/S105381191830380X [Accessed January 15,
705 2019].

706 Stephan KE, Iglesias S, Heinzle J, Diaconescu AO (2015) Translational Perspectives for Computational

Neuroimaging. Neuron 87:716–732 Available at: https://www.sciencedirect.com/science/article/pii/S0896627315006303 [Accessed February 26, 2019].

Stephan KE, Kasper L, Harrison LM, Daunizeau J, den Ouden HEM, Breakspear M, Friston KJ (2008) Nonlinear dynamic causal models for fMRI. Neuroimage 42:649–662 Available at: https://www.sciencedirect.com/science/article/pii/S1053811908005983 [Accessed February 26, 2019].

Sukov W, Barth DS (2001) Cellular mechanisms of thalamically evoked gamma oscillations in auditory cortex. J Neurophysiol 85:1235–1245 Available at: http://www.physiology.org/doi/10.1152/jn.2001.85.3.1235 [Accessed June 18, 2018].

Symmonds M, Moran CH, Leite MI, Buckley C, Irani SR, Stephan KE, Friston KJ, Moran RJ (2018) Ion channels in EEG: isolating channel dysfunction in NMDA receptor antibody encephalitis. Brain 141:1691–1702 Available at: https://academic.oup.com/brain/article/141/6/1691/4990439 [Accessed July 8, 2019].

Whittington M., Traub R., Kopell N, Ermentrout B, Buhl E. (2000) Inhibition-based rhythms: experimental and mathematical observations on network dynamics. Int J Psychophysiol 38:315–336.

Whittington MA, Cunningham MO, LeBeau FEN, Racca C, Traub RD (2011) Multiple origins of the cortical gamma rhythm. Dev Neurobiol 71:92–106 Available at: http://doi.wiley.com/10.1002/dneu.20814 [Accessed September 4, 2018].

Wu X, Huang L, Wu Z, Zhang C, Jiang D, Bai Y, Wang Y, Chen G (2013) Homeostatic competition between phasic and tonic inhibition. J Biol Chem 288:25053–25065 Available at: http://www.ncbi.nlm.nih.gov/pubmed/23839941 [Accessed June 27, 2018].

Wyss C, Tse DHY, Kometer M, Dammers J, Achermann R, Shah NJ, Kawohl W, Neuner I (2017) GABA

731 metabolism and its role in gamma-band oscillatory activity during auditory processing: An MRS
732 and EEG study. Hum Brain Mapp 38:3975–3987 Available at:
733 http://www.ncbi.nlm.nih.gov/pubmed/28480987 [Accessed February 26, 2019].

734 Zeidman P, Jafarian A, Seghier ML, Litvak V, Cagnan H, Price CJ, Friston KJ (2019) A guide to group
735 effective connectivity analysis, part 2: Second level analysis with PEB. Neuroimage 200:12–25
736 Available at: https://www.sciencedirect.com/science/article/pii/S1053811919305233
737 [Accessed October 9, 2019].

738

739

Figure Legends

Figure 1. The neuronal model.

a. Intrinsic connectivities found in all nodes between layer 4 stellates (ss), inhibitory interneurons (ii), superficial pyramidal modules (sp) and deep pyramidal modules (dp).

b. All 6 nodes used are represented as a network on the left, showing the extrinsic connectivities (solid line = forward; dotted line = backward; dashed line = lateral). A left hemisphere representation of these bilateral nodes in primary auditory cortex, superior temporal gyrus and inferior-frontal gyrus (light, medium and dark grey, respectively).

c. A detailed view of the extrinsic population connections for forward (solid lines) and backward (dotted lines) connections.

d. Matrices of the extrinsic and intrinsic connectivity weights, all of which had a permitted variance of 1/16.

e. A process flow describing the steps taken in the meta-analysis phase.

Figure 2. Event Related Fields (ERFs).

a. Mean ERFs across all subjects for all six nodes for the standard and deviant trials from 0-380ms. The difference wave (MMN) is also shown. ERFs from the placebo condition are shown in blue and from the tiagabine condition in red. Significant changes with time across the drug condition are shown as a thick black line within each axis ($p<0.05$, Bonferroni corrected for 6 regions). Shaded areas represent the standard error (SEM).

b. Significant differences for induced spectra power were found in the alpha (α), beta (β) and lower and higher gamma bands (γ1 and γ2) (FWE cluster corrected at $p<0.001$). Here they are shown as flat scalp maps (lower plots) with rostro-caudal activity *versus* time (upper plots). The time axis runs from 0–380 ms post-stimulus.

c. Source-reconstructed T-contrasts ($p<0.001$) created for those frequency bands showing spatial changes across the drug condition in the 135 – 235 ms time window.

Figure 3. Comparison between model and data.

a. Residual differences between the observed and model-generated ERFs are shown for both the standard 4-cell conductance-based DCM and the ext-DCM. ERFs from all nodes for every subject are concatenated along the y-axis.

b. Bayesian model comparison of the 4-cell conductance-based DCM and the ext-DCM favours the ext-DCM, plotted here in terms of the posterior model probability (RFX Bayes Factor = 40.6).

c. Predicted ERFs are shown for the standard and deviant conditions, along with the difference wave (Std–Dev). The placebo and tiagabine conditions are depicted in blue and red respectively with significant differences ($p<0.05$, Bonferroni corrected for 6 regions) shown as a thick black line within each axis.

d. Correlation coefficient between prediction and data for each node and each condition. Boxplots represent the distribution over subjects with small dots representing outliers and larger black circles representing the correlation coefficient of the meaned response of all subjects for each node and each condition.

Figure 4. Prediction of hidden states.

a. Significant differences in the modulation of GABA-A synaptic scaling for each of the three symmetric nodes. Green/red show significantly greater/lesser GABA-A synaptic scaling for tiagabine than the placebo. Posterior probability p-values are shown next to each connection.

b. To explore the functional differentiation between regions during the task conditions with respect to tonic inhibition, tonic GABA-A scaling on deep interneurons in IFG, STG and Aud, for each

individual is plotted for the placebo and tiagabine conditions. The standard and deviant conditions are plotted separately in the left and right columns respectively. Pair-wise Bayesian t-test statistics are reported on each plot, showing the Bayes Factor for each of the 6 comparisons. When there is evidence for a difference, or evidence for no difference, the Bayes factor is shown in green or blue respectively.

c. The correlation demonstrates the dynamic balance that persists between phasic and tonic inhibition (see main text discussion). Linear fit with 95% confidence bounds for tonic GABA-A scaling on deep inhibitory neurons vs phasic GABA-A scaling from deep inhibitory neurons to thalamic projecting pyramidals (Bayesian correlation pairs, Bayes factor=398.43).

Table 1. Model parameters.

Parameter values used by the neuronal model are shown with their permitted variances.

Parameter grouping	Parameter	Initial value	Permitted variance
Decay Constants, τ (ms)	AMPA τ	4	1/16
	NMDA τ	100	1/16
	GABAA τ	16	1/8
	GABAB τ	200	1/8
	I_M τ	160	0
	I_H τ	100	0
Misc. strengths	K^+ leak G	1	0
	Background V	2.17	1/32
Reversal potentials (mV)	Na^{2+} reversal	60	0
	Ca^{2+} reversal	10	0
	Cl^- reversal	-90	0
	K^+ reversal	-70	0
	I_H reversal	-100	0
Firing threshold (mV)	V_T (all pops)	-40	0
Firing precision	V_X (all pops)	1	1/32
I_H I-V slope	V_{HX}	300	0
Cell Capacitances (pF)	ss_C	200	1/32
	sp_C	150	1/32
	si_C	50	1/32
	dp_C	400	1/32
	di_C	50	1/32
	tp_C	200	1/32
Delays (ms)	intrinsic	2	1/32
	extrinsic cortico-cortical	16	1/32
	extrinsic thalamo-cortical	80	1/32

Table 1

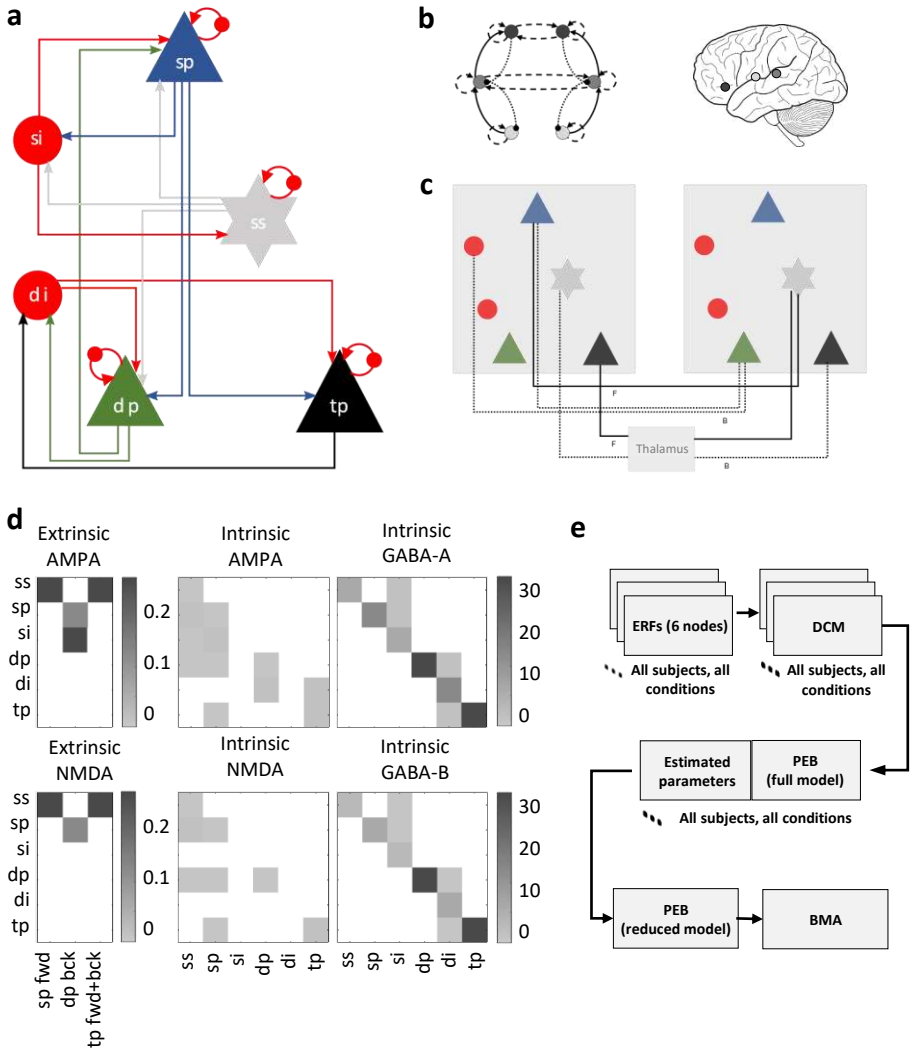
a
sp
si
ss
d i
d p
tp
b
c
F
B
F
B
Thalamus
d
Extrinsic AMPA
Intrinsic AMPA
Intrinsic GABA-A
Extrinsic NMDA
Intrinsic NMDA
Intrinsic GABA-B
ss
sp
si
dp
di
tp
0.2
0.1
0
30
20
10
0
sp fwd
dp bck
tp fwd+bck
e
ERFs (6 nodes)
DCM
All subjects, all conditions
All subjects, all conditions
Estimated parameters
PEB (full model)
All subjects, all conditions
PEB (reduced model)
BMA

Figure 1

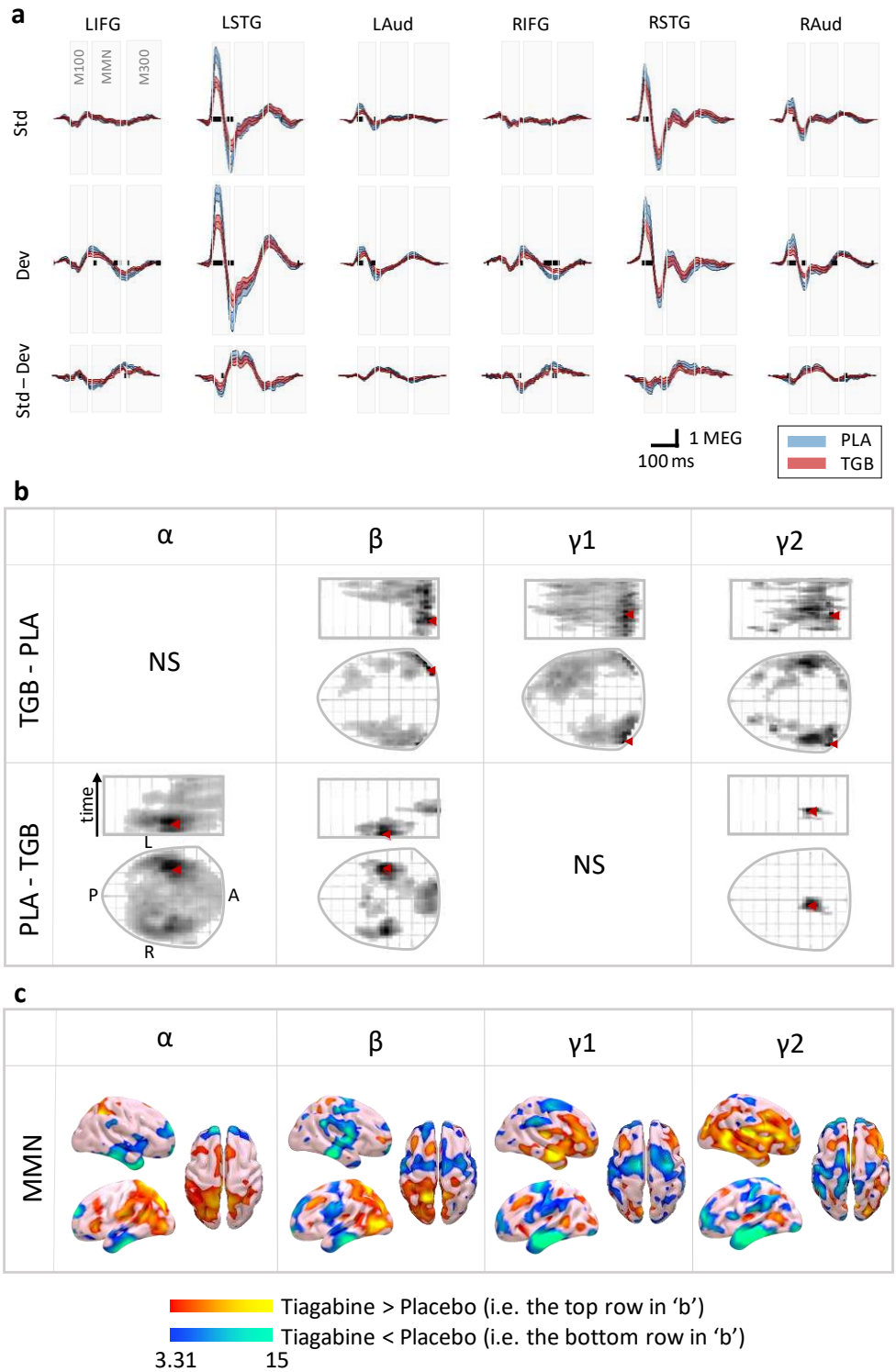
a
LIFG
LSTG
LAud
RIFG
RSTG
RAud
M100
MMN
M300
Std
Dev
Std – Dev
1 MEG
100 ms
PLA
TGB
b
α
β
γ1
γ2
TGB - PLA
NS
PLA - TGB
time
L
P
A
R
NS
c
MMN
Tiagabine > Placebo (i.e. the top row in 'b')
Tiagabine < Placebo (i.e. the bottom row in 'b')
3.31
15

Figure 2

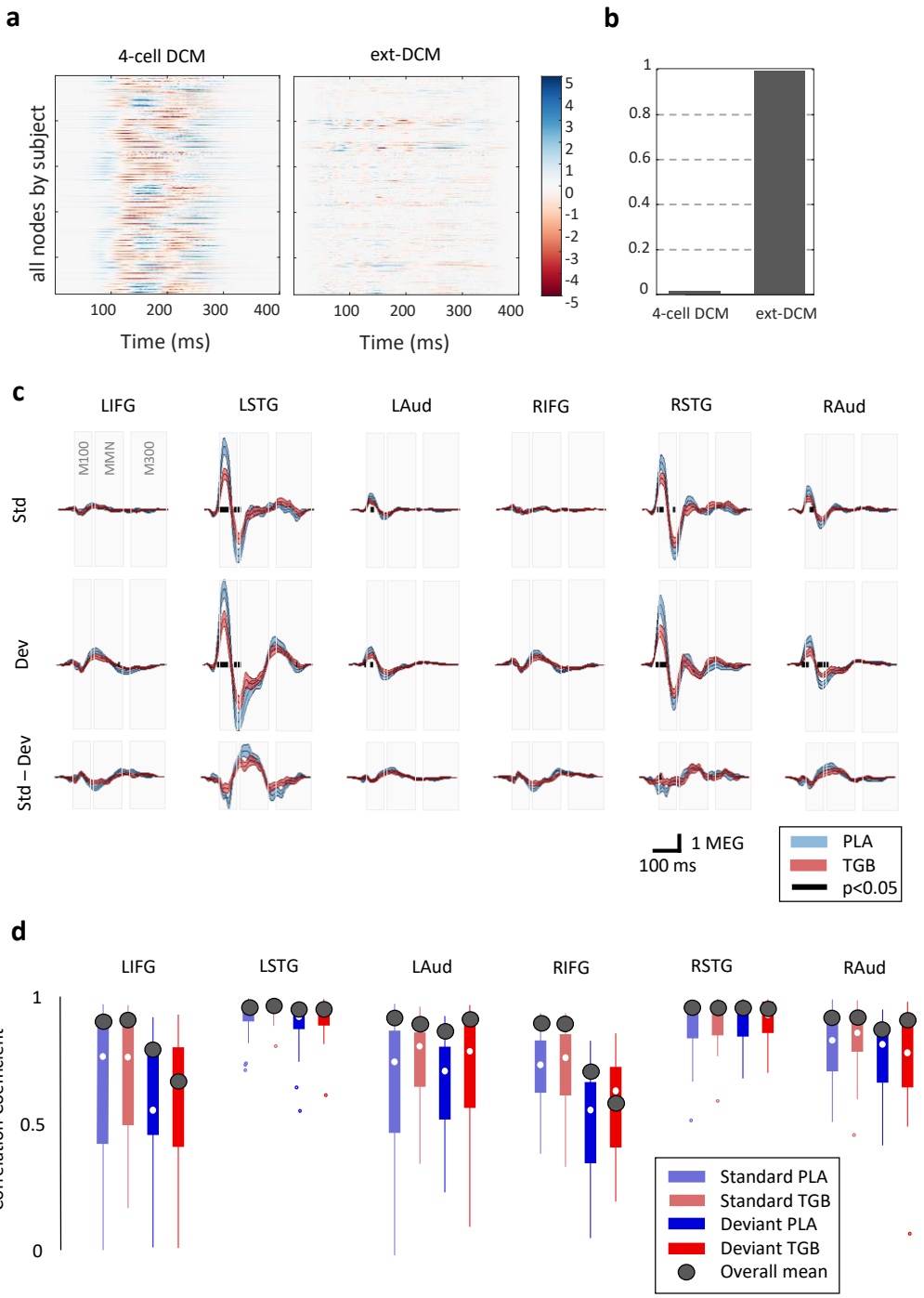
a
4-cell DCM
ext-DCM
all nodes by subject
100 200 300 400
Time (ms)
100 200 300 400
Time (ms)
5 4 3 2 1 0 -1 -2 -3 -4 -5
b
1 0.8 0.6 0.4 0.2 0
4-cell DCM
ext-DCM
c
LIFG
LSTG
LAud
RIFG
RSTG
RAud
M100
MMN
M300
Std
Dev
Std – Dev
1 MEG
100 ms
PLA
TGB
p<0.05
d
LIFG
LSTG
LAud
RIFG
RSTG
RAud
Correlation Coefficient
1
0.5
0
Standard PLA
Standard TGB
Deviant PLA
Deviant TGB
Overall mean

Figure 3

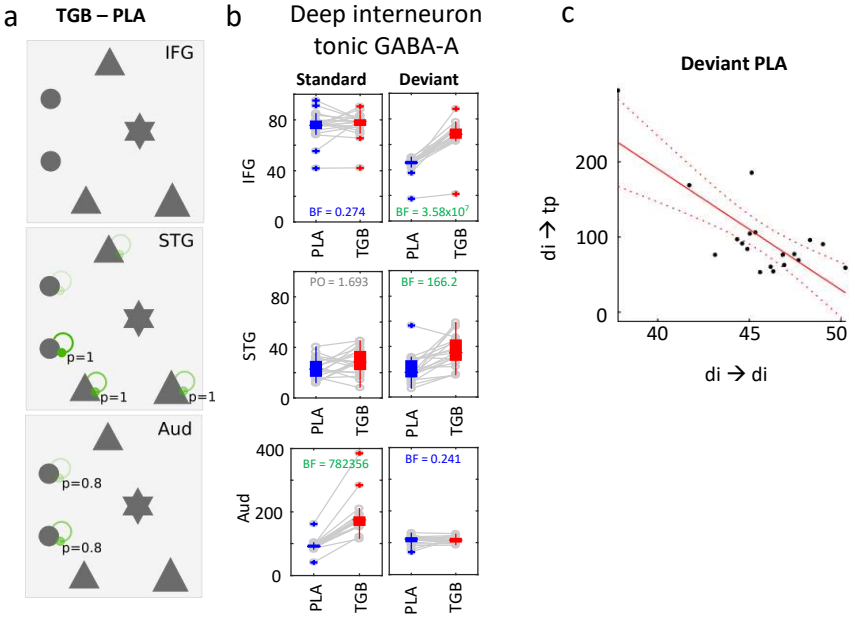
a
TGB – PLA
IFG
STG
Aud
p=1
p=1
p=1
p=0.8
p=0.8
b
Deep interneuron
tonic GABA-A
Standard
Deviant
IFG
STG
Aud
BF = 0.274
BF = 3.58x10^7
PO = 1.693
BF = 166.2
BF = 782356
BF = 0.241
PLA
TGB
c
Deviant PLA
di → tp
di → di

Figure 4